Materials Transactions, Vol. 44, No. 11 (2003) pp. 2288 to 2297

Low Temperature Superplasticity and Its Deformation Mechanism in Grain Refinement of Al-Mg Alloy by Multi-Axial Alternative Forging*[1]

Masafumi Noda[1,*2], Mitsuji Hirohashi[2] and Kunio Funami[3]

[1]*Department of Artificial System Science and Engineering, Graduate School of Science and Technology, Chiba University, Chiba 263-8522, Japan*
[2]*Department of Electronics and Mechanical Engineering, Chiba University, Chiba 263-8522, Japan*
[3]*Department of Mechanical Engineering, Chiba Institute of Technology, Narashino 275-0016, Japan*

In practical application, an appearance of low temperature superplasticity (LSTP) is one of necessaries conditions. In this paper, to estimate an appearance and deformation mechanisms of this superplasticity, the role of grain boundary sliding (GBS), intragranular deformation and the change of microstructure during superplastic deformation have been investigated for ultrafine-grained Al-Mg alloy with a grain size of less than 1 μm using Multi-Axial Alternative Forging (MAF) technique. In these materials, it shows that the elongation and strain rate sensitivity (m-value) were 340% and 0.39, respectively, at 473 K under a strain rate of 2.8×10^{-3} s^{-1}. These results show that superplastic appearance is possible at 473 K. The void formed at 473 K elongated in parallel to the tensile direction, with a length of 15 μm and a width of 5 μm. The intragranular deformation contribution was estimated from the aspect ratio of the grains after deformation and its contribution ratio was about 33.5 %. Therefore, for the appearance of lower temperature superplasticity with large elongation and m-value, the role of intragranular deformation was the most important factor together with GBS under these conditions. As described above, the MAF technique is one of the most effective methods to produce ultrafine-grained material and appearance of lower temperature superplasticity.

(Received May 29, 2003; Accepted September 30, 2003)

Keywords: *low temperature superplasticity, ultrafine grain, intragranular deformation, grain boundary sliding, void, multi-axial alternative forging, aluminum-magnesium alloy*

1. Introduction

Improved grain refinements techniques have resulted in create of Al alloys with an ultrafine grain structure. It was well known that one of the demands as appearance of low-temperature superplasticity using these materials[1–9] that ultrafine grain materials are effective in helping to achieve low-temperature superplasticity (LTSP), but most discussions up to now, on appearance of LTSP in ultrafine grain Al alloys are based on the results of tensile test temperature at 673 K.[5–9] This temperature is higher than the recrystallization temperature of Al alloy, and it has been reported that the grain growth is occurred before reaching this test temperature.[10–14] Ultrafine grain materials are consequently affected by coarsening before deformation. It is shown, to carry out the experimental and examination, which eliminated the influence of grain growth are necessary for the argument on a deformation mechanism.

Grain boundary sliding (GBS) was important role in the deformation mechanism that appearance of superplasticity.[15–20] The contribution ratio of GBS under conditions where superplasticity noticeably appears in various Al alloys is reported to be about 70 to 80%.[18–20] There are, however, only a small number of reports that discuss how the contribution ratio may be related to the ultrafine grain materials used and the test temperature. It is necessary to study structural changes at much lower temperatures to clarify the deformation mechanisms at LTSP.

In the present study, as in those we have previously reported,[21,22] Al-Mg alloys were used that had been processed using multi-axial alternative forging (MAF), a technique that enables the creation of ultrafine grain materials. The tensile test carried out at different strain rates at 473 K and 673 K. The deformation mechanism of LTSP was examined from the structural changes before and after deformation.

2. Experimental Method

The material used was Al-Mg alloy. Its chemical composition in mass% was 0.10 Si, 0.20 Fe, 0.02 Cu, 0.64 Mn, 4.54 Mg, 0.12 Cr, and 0.02 Ti, with the balance as Al. The cast Al-Mg alloy material was given a homogenizing thermal treatment at 853 K for 28.8 ks, resulting in the formation of equiaxial grains 67 μm in diameter. The material was machined into cubic blocks with sides of 50 mm for use as test samples, which were then further treated using the MAF process as shown in Fig. 1. The length, width and thickness of the samples were defined as L, LT and ST, respectively. The MAF process involved application of repeated forging to each test sample from three axial directions per pressing while rotating it at 90° so that a true strain of 6.0 was applied. The test samples were heated to 543 K and kept for 3.6 ks; meanwhile, a forging reduction ratio of 20% relative to the original plate thickness was applied per pressing. After each pressing treatment, the test samples were reheated and kept at 543 K for 1.2 ks, then finally water-quenched.

Tensile specimens with gauge dimension of 3 mm in length, 3 mm in width, and 1 mm in thickness, were carved out of the L - LT surface of the MAF samples. The longitudinal direction of the specimen and the L direction of the sample material were parallel. The final forging direction and the specimen surface from which the specimens were carved had no impact on the differences in the tensile

*[1]This Paper was Originally Published in Japanese in J. Japan Inst. Metals **67** (2003) 98-105.
*[2]Graduate Student, Chiba University

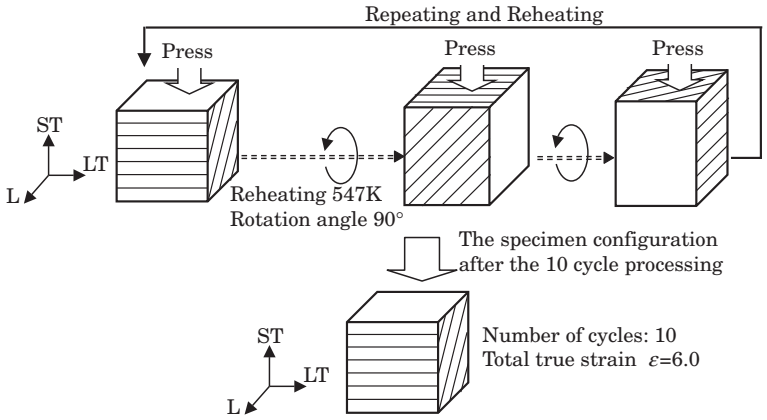

Fig. 1 Schematic illustration of the working process for the multi-axial alternative forging.

test results.[9,21,22] Tensile tests were carried out at 473 K and 673 K and at a strain rate ($\dot{\varepsilon}$) of 2.8×10^{-4} to $2.8 \times 10^{-1}\,s^{-1}$. At the test temperature of 473 K, it was confirmed that the grain size of 1 μm or less had been maintained to just before the tensile test. Thus, it was decided to set the test temperature at 473 K to clarify the deformation behavior under LTSP of the ultrafine grain material. The specimens were heated to the test temperature at $0.17\,Ks^{-1}$. After the specimens reached the test temperature, they were maintained in that state for 0.9 ks. After the tensile test, the specimens were furnace-cooled. The microstructure of the material after deformation was observed by optical microscopy, SEM and TEM. Fracture surfaces were observed by SEM. TEM observation was carried out on the specimens at an acceleration voltage of 200 kV after they had been machine-polished and wrought into thin foil by high-speed ion polishing. Grain size was measured by the intercept method.[23]

3. Experimental Results

3.1 Create of ultrafine grain by MAF and changes in microstructure by thermal treatment

Figure 2 shows TEM microstructure of the MAF material, Inverse Pole Figure (IPF) maps obtained from EBSP analysis, and histograms of the grain boundary misorientations. The L-LT plane of the specimens was observed by TEM and subjected to EBSP analysis in steps of 0.1 μm with the IPF map determined by the standard triangle shown in the figure. Selected diffraction patterns shown in Fig. 2(a) were obtained from areas in which 2 μm in diameter were present. As can be seen in Fig. 2(a), the typical diffraction pattern is ring-shaped, indicating that it is a multicrystalline material. In the IPF map shown in Fig. 2 (b), the MAF material was not completely recrystallized, and, even after the above treatment, contained some unrecrystallized structures. However, it should be noted that no strong texture was seen in any specific direction. As shown in Fig. 2 (c), high-angle grain boundaries were found in 70% of the measured field of view. Regarding the difference in grain boundary misorientation, angles between 2° and 15° and those of 15° or more were defined as low-angle and high-angle grain boundaries, respectively.

Figure 3 shows observations by optical microscope and TEM of the samples heated to the test temperatures of 473 K and 673 K kept for 0.9 ks, and water-quenched. Hereinafter referred to as "473 K samples" and "673 K samples" respectively. Those in Fig. 3 all correspond to the microstructure observed immediately before the tensile test. The mean grain size was 0.8 μm and 10 μm in the 473 K samples and 673 K samples, respectively. In the 673 K samples, recrystallization was already completed before deformation, indicating that grain growth had occurred.

3.2 Appearance of superplastic behavior

Nominal stress-strain curves for the 473 K and 673 K samples at $\dot{\varepsilon} = 2.8 \times 10^{-1}$ to $2.8 \times 10^{-4}\,s^{-1}$ are shown in Fig. 4, and the peak stress and total elongation curves plotted relative to $\dot{\varepsilon}$ are shown in Fig. 5 together with the strain rate sensitivity exponent (m-value). As indicated in Figs. 4 and 5, the maximum stress decreased with the appearance of superplasticity under all test conditions. What is noteworthy is that a total elongation with an m-value of 0.39, representing an increase of 340%, was achieved even in the 473 K samples at $2.8 \times 10^{-3}\,s^{-1}$. A rough indicator of the appearance of superplasticity in the past has been considered to be an m-value of 0.3 or more and an elongation of about 200%.[15–17] This research result satisfied these deformation conditions. For $\dot{\varepsilon} = 2.8 \times 10^{-3}\,s^{-1}$, total elongation shows almost the same value in both the 473 K and 673 K samples, with their respective m-values being 0.39 and 0.35. It is inferred that the test temperature made a difference in the contribution ratio of GBS and that of intragranular deformation.

3.3 Microstructure change associated with tensile deformation

TEM and SEM microstructure near the fractured parts of the specimens that failed at 473 K and 673 K at $\dot{\varepsilon} = 2.8 \times 10^{-3}\,s^{-1}$ are shown in Fig. 6. Crystal grains grew from 10 to 25 μm during deformation in the 673 K samples. As discussed in previous reports,[4,24] the deformation of 673 K samples is characterized by significant rotation of crystal grains and GBS, from which it is deduced that dynamic recrystallization and grain growth play a major role. In the 473 K samples, on the other hand, crystal grains were elongated in the tensile direction 0.8 μm in width (D_{LT}) and

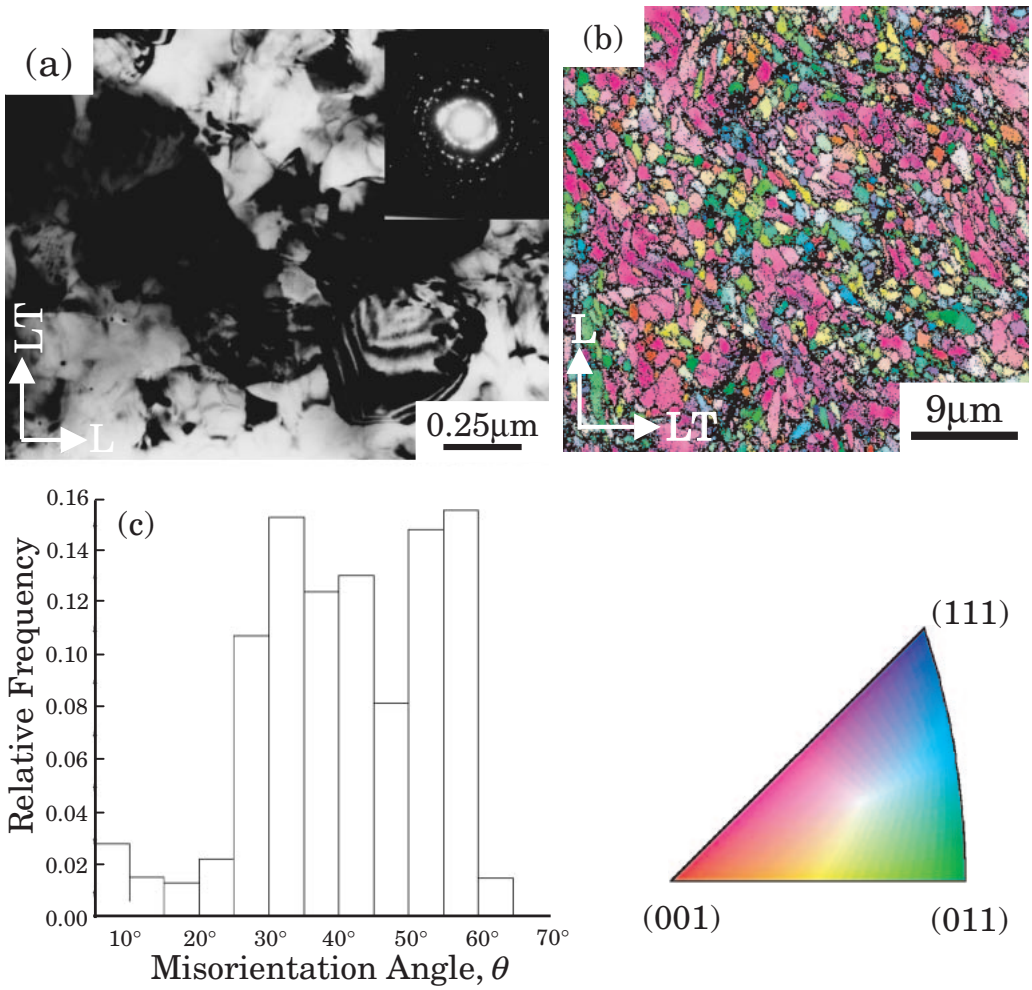

Fig. 2 Microstructure and EBSP analytical result of the MAFed material. (a) TEM microstructure, (b) IPF map and (c) Frequency histogram of misorientations angle. The high-angle grain boundaries whose misorientations are larger than 15 degree was defined.

1.7 μm in length (D_L). However, since the specimens were furnace-cooled down to 323 K after the test, it is possible that the microstructure was somehow recovered in the 473 K samples under the cooling conditions. Figure 7 shows TEM microstructure when the specimens that fractured at 473 K and $2.8 \times 10^{-3}\,s^{-1}$ were water-quenched. Water-quenching was carried out within 30 s of completion of the test. Dislocation of the grains occurred to a greater extent than that seen in Fig. 6(b), and dislocations was concentrated near the grain boundaries. At that time, D_{LT} was 0.78 μm and D_L was 1.9 μm, showing that re-arrangement and disappearance of dislocations occurred due to recovery of the material during furnace-cooling and that grains were transformed from subgrains to crystal grains with clear grain boundaries. However, crystal grains were elongated after furnace-cooling and dislocations were still evident inside the grains. In other words, judging from the shape of the crystal grains before and after deformation and the existence of intragranular dislocations, it is inferred that intragranular deformation contributed to deformation of the material in the 473 K samples. Comparing Fig. 3 with Fig. 6, although dislocations were formed in grains in the 473 K samples, the crystal grains did not markedly coarsen; instead, they maintained a fine structure.

To investigate the microstructure change associated with low-temperature deformation, 50% and 150% tensile deformation was applied to the specimens at 473 K and $2.8 \times 10^{-3}\,s^{-1}$. TEM microstructures after tensile deformation are shown in Fig. 8, and the mean grain size in the tensile direction and the vertical direction and the aspect ratio (AR) are shown in Table 1 as a rough indicator of intragranular deformation. Upon 50% deformation, dislocations were already formed in grains and AR changed from 1.0, immediately before deformation, to 1.3 after deformation. After 150% deformation, AR became 1.5 and the grain size showed no major change in the width direction but was elongated in the tensile direction. Subsequently, AR increased from 1.5 to 2.1 before reaching fracture, representing double the value immediately before deformation. From these results, it is considered that tensile deformation in the 473 K samples is characterized by a greater contribution of intragranular deformation than is seen in the 673 K samples.

Other ultrafine grain materials were tested at 673 K for the Al alloy of 3% Sc and 0.2% Mg ($\dot{\varepsilon} = 3.3 \times 10^{-2}\,s^{-1}$)[5] and Al-Mg alloy ($\dot{\varepsilon} = 1.7 \times 10^{-3}\,s^{-1}$).[8] The results were as follows: (1) crystal grains grew while maintaining their equiaxial condition before and after deformation; (2) cracks were observed during deformation, which were caused by GBS; and (3) voids had an equiaxial shape of a few tens of μm. These findings indicate that the results of experiments in

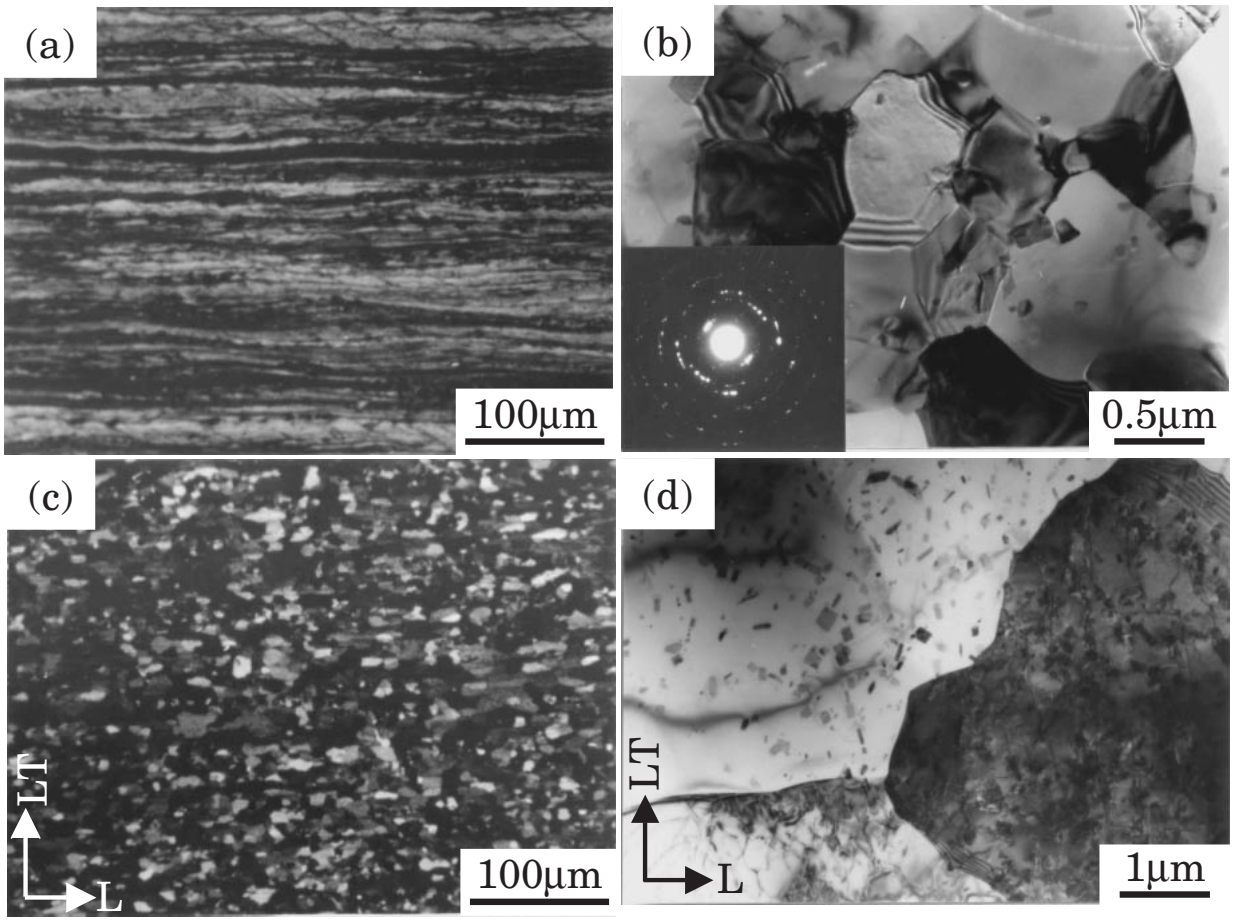

Fig. 3 Optical and TEM microstructures just before tensile test at (a),(b) 473 K and (c),(d) 673 K. Tensile specimens were heated at each temperature with a heating ratio of 0.17 Ks^{-1} and held for 0.9 ks.

the present study with respect to internal microstructure change agree with the results of the previous reports on experiments conducted at 673 K although there is a difference in strain rate. On the other hand, the results of the experiment in the 473 K samples include the following: (1) the shape of crystal grains changed from equiaxial to elongated as deformation occurred, with no extreme grain growth appearing; (2) dislocations formed in grains after deformation, with no cracks found along the grain boundaries; and (3) voids elongated parallel to the tensile direction. In summary, observation of the internal microstructure of the specimens revealed a great difference in microstructure change associated with the progress of deformation between 673 K and 473 K.

3.4 Formation of voids

In the SEM microstructure shown in Fig. 6, large equiaxial voids of about 62 μm are observed near the fractured portion in the 673 K samples. On the other hand, voids formed at 473 K are elongated in the tensile direction and their size is about 5 μm in width and 15 μm in length. From the TEM observations in shown Figs. 3, 6 and 8, it can be seen that there was no change in D_{LT} before and after deformation, with the size mostly remaining at 0.8 μm. D_{LT} showed no change despite deformation until fracture, probably because microstructure modification occurred due to recovery during deformation or furnace-cooling as explained earlier. On the other hand, D_L changed from 1.0 to 1.7 μm after deformation and elongated in the tensile direction. Crystal grains and voids both elongated, presumably due to the major contribution of intragranular deformation. In the 673 K samples, the voids grew in the direction normal to the tensile direction as reported earlier.[5–8,11)]

4. Discussion

4.1 Effect of test temperature on grain boundary sliding and intragranular deformation

The appearance of superplasticity in the material heated to 473 K indicates a high contribution of intragranular deformation. In general, the major deformation mechanism of the appearance of superplasticity is thought to be GBS.[16–20)] The contributions of test temperature and intragranular deformation were studied next. Alumina powder with particles size 0.3 μm in diameter was used to scratch the surface of test specimens before deformation was applied to the specimens and the microstructure of scratched line after 10% and 50% deformation were observed. Figure 9 shows the SEM microstructure (a) and (b) in the 473 K samples and (d) to (e) in the 673 K samples. Figures 9(c) and (f) are magnified images of (b) and (e). The scratches were linear when predeformation was given 10%. After 50% deformation, however, in (c) they are curved in a wavelike pattern in grains, and in (f) they are linear in grains, with their gradient changed

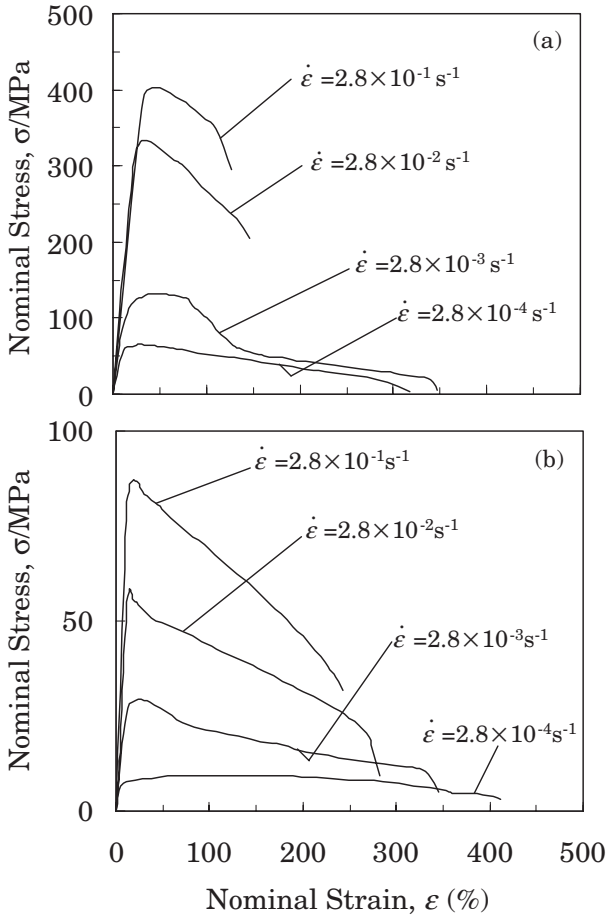

Fig. 4 Nominal stress-strain curves of the MAFed materials at (a) 473 K and (b) 673 K with various strain rates.

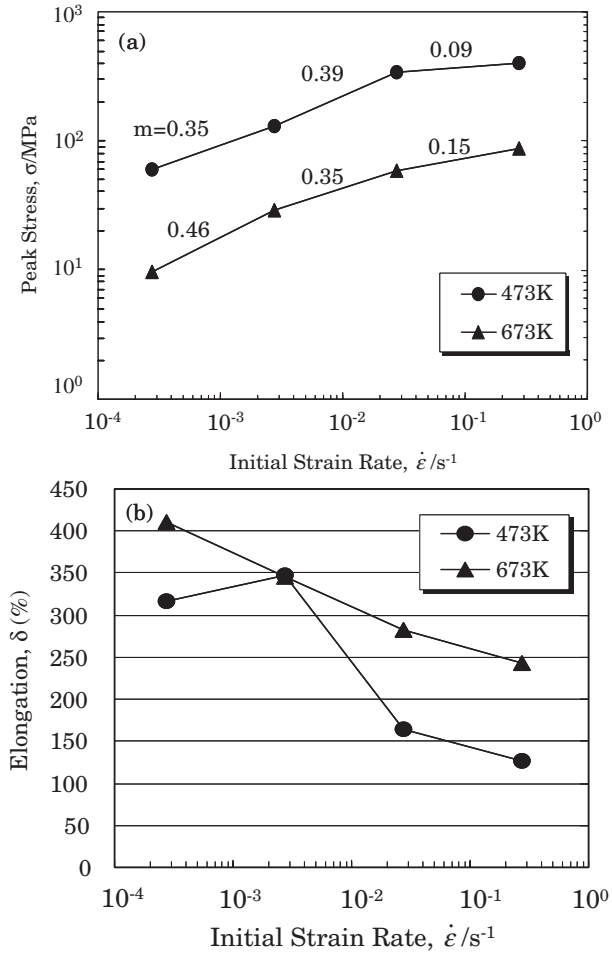

Fig. 5 Strain rate dependence of the peak stress (a) and total elongation (b) of the MAFed materials. The strain rate sensitivity (m-value) is shown in (a).

at grain boundaries. The grain is elongated in 473 K samples, as is clearly from the high resolution SEM microstructure in Fig. 10. It was clearly recognized that the contribution of GBS and formation of voids along with intragranular deformation interact each other for the deformation. In Figs. 9(c) and 10, crystal grains are elongated to the tensile direction, while in Fig. 9(f) the equiaxial grains were maintained. It is inferred that intragranular deformation due to dislocational movement and GBS was the main deformation mechanism of superplastic deformation in the 473 K and 673 K samples, respectively. Curved scratches as shown in Fig. 9(c) are generally observed when the contribution rate of GBS is very small, with an m-value of less than 0.3.[10,20,25] However, such scratches also occurred in the 473 K samples at an *m*-value of 0.39, and this phenomenon corresponds with the observation shown in Fig. 6(b) and Fig. 8 in which dislocations were present. This indicates that the contribution ratio of intragranular deformation is greater than that seen in the 673 K samples.

Scratch deviation occurs at grain boundaries due to GBS. The angle θ of scratches at grain boundaries are likely to provide a guideline for GBS.[18] At the same time, although the degree of deviation angle θ cannot measure anti-plane sliding as sliding normal to the surface, it is inferred that the degree corresponds to the in-plane sliding at grain boundaries. Here, θ was evaluated from two-dimensional photos of the specimen microstructure and 100 arbitrarily chosen crystal grains on the surface of the test specimen after 50% deformation was measured, as shown in Fig. 11, to calculate the average of the measured values. The GBS angle θ is 4.3° in the 473 K samples, whereas it is 25° in the 673 K samples, indicating the occurrence of considerable sliding and rotation of crystal grains during deformation. For 50% deformed samples, GBS was greater for deformation in the 673 K samples than in the 473 K samples, which is obvious from the value of θ obtained. It is reported that the sloping direction of scratches corresponds to the direction of GBS.[20,25] Since the slip of scratches frequently occurs at grain boundaries, it is inferred that the deformation mechanism in the 673 K samples is based on GBS.

Next, the contribution ratio of intragranular deformation was evaluated from the AR of crystal grains before and after deformation.[26–28] AR was obtained from measurements of D_L and D_{LT} grain size that were obtained from the SEM and TEM microstructure of the specimen with 50% deformation. The contribution of intragranular deformation (ε_g) and GBS (ε_{gbs}) to the total elongation were calculated by the following equation,[18,20,25,26] respectively. R_0 and R were shown in equation[25,26,28] (1) are the AR before and after deformation. The nL shown in the equation[18,20,29] (2) is the number of grain boundary which intersects the scratch of unit length. The $\bar{u}_t$ is the average of u_t as shown in Fig. 11 and $\bar{u}_t$ was

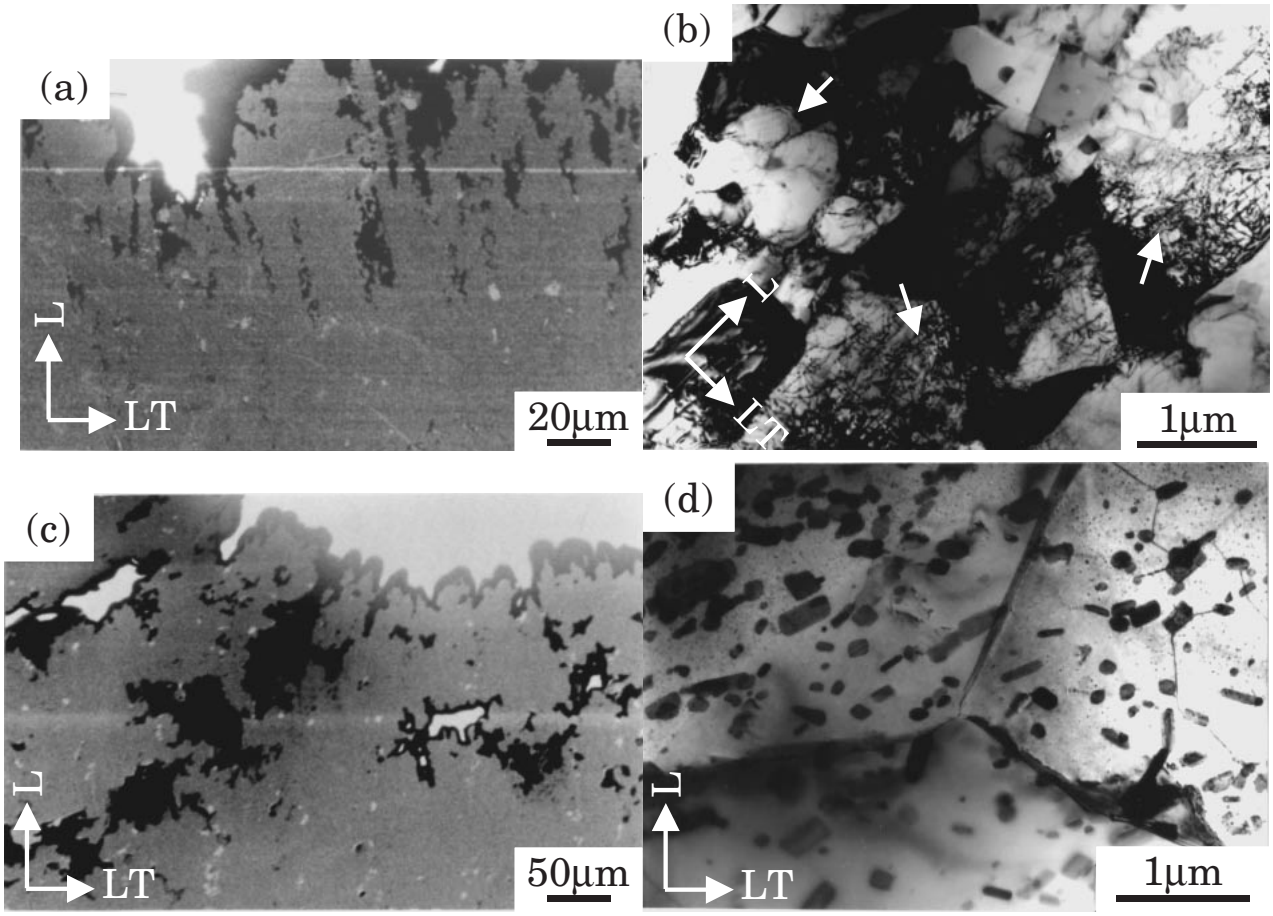

Fig. 6 SEM and TEM microstructures near the fracture tips after deformation at (a)(b) 473 K and (c)(d) 673 K with strain rate of $2.8 \times 10^{-3}\,s^{-1}$.

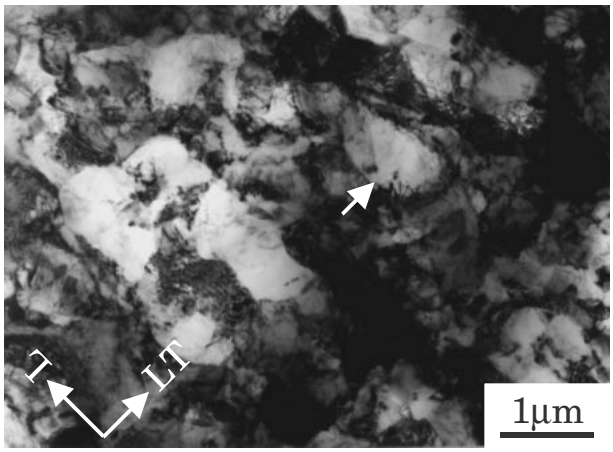

Fig. 7 TEM microstructure of water quenched after tensile test. Water quenching was carried out within the 30 second after the tensile specimen has broken.

rectified using the degree of deviation angle θ. Where the ε_t shows the total strain given in order to calculated for the aspect ratio. The results showed that the contribution ratio of intragranular deformation was about 33.5% in the 473 K samples and about 14.4% in the 673 K samples. The value of the 473 K samples was about 2.3 times greater than that of the 673 K samples. On the other hands, the contribution ratio of grain boundary sliding to be about 28% in the 473 K samples and about 70% in the 673 K samples.

$$\varepsilon_g = 1 - (R_0/R)^{(2/3)}/\varepsilon_t \quad (1)$$

$$\varepsilon_{gbs} = (1 + \varepsilon_t) n_L \bar{u}_t/\varepsilon_t \quad (2)$$

It has been reported that the contribution ratio of intragranular deformation was 16% when 7075Al alloy was tested at 673 K and $1.7 \times 10^{-3}\,s^{-1}$[24] and that it was 15 to 20% when Al-Zn-Mg alloy and Al-Mg alloy were tested at 733 K and $3.0 \times 10^{-3}\,s^{-1}$ and $1.1 \times 10^{-3}\,s^{-1}$, respectively.[18–20] A comparison of these reports with our results for the 673 K samples shows good agreement between the values. Thus, it is conclude that even when intragranular deformation is main deformation mechanisms, large elongation or high m-value can be obtained. In other words, superplastic deformation at 473 K and $2.8 \times 10^{-3}\,s^{-1}$ was more significantly affected by intragranular deformation than that at 673 K, which means that dislocational movement in grains actively occurred during deformation. We consider this to be closely related to GBS, possible to obtain greater elongation and a larger m-value.

It is thought that the remainders of the balance contribution ratio to total elongation are formation of void and diffusion as a factor of the deformation mechanism of superplasticity.[16–20] However, in this study, contributions of void or diffusion to a deformation mechanism have not been understood.

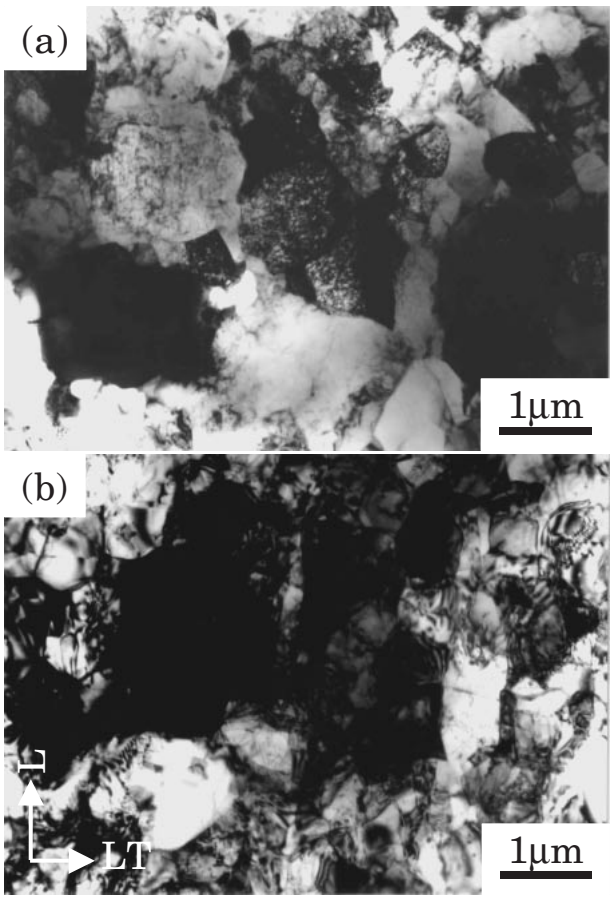

Fig. 8 TEM microstructures obtained at the center of the gauge length after deformation at 473 K, with strain rate of $2.8 \times 10^{-3}\,s^{-1}$. Elongated to (a) 50% and (b) 150%.

Table 1 Relationship between aspect ratio and average grain size D_L and D_{LT} after deformation with strain rate of $2.8 \times 10^{-3}\,s^{-1}$ under various deformed ratio. (a) 473 K and (b) 673 K.

(a)	Just before tensile test	50%	150%	250%
D_{LT}(μm)	0.82	0.82	0.82	0.83
D_L(μm)	0.80	1.06	1.25	1.73
Aspect ratio	0.98	1.29	1.52	2.1
(b)	Just before tensile test	50%	150%	250%
D_{LT}(μm)	10.01	10.34	11.18	13.83
D_L(μm)	9.92	11.64	13.38	20.47
Aspect ratio	1.01	1.13	1.2	1.48

4.2 Microstructure change during the appearance of superplasticity

GBS is the main deformation mechanism in superplasticity, the subgrain structure shown in Figs. 6 and 8 will not, in general, be formed.[4,24,30] The TEM microstructure of the specimens after deformation at 473 K and $2.8 \times 10^{-3}\,s^{-1}$ shown in Figs. 6 and 8 demonstrate that dislocations were formed in crystal grains with the increase in deformation, eventually transforming into subgrains, and crystal grains elongated in the tensile direction. Elongated grains and equiaxial fine grains (as identified by the arrows in the figures) were also observed. As discussed above, the specimens had dislocations in the grains at a GBS angle of $\theta = 4.3^\circ$ in the 473 K samples. Therefore, the existence of subgrains confirmed in Fig. 7 suggests that subgrains contribute in a minor way to sliding and rotation. According to Sakai *et al.*,[4,24,31] the relationship between internal structure, rotation of crystal grains and GBS is explained by the occurrence of local GBS and rotation of subgrains, transforming low-angle grain boundaries changed to high-angle grain boundaries and forming new fine grains in high-strain ranges; dynamic recrystallization is also reported to be a contributing factor. High-strain ranges in this case correspond to fewer than 150% deformation. Top surface observation of the specimens by SEM showed that all grains in the observed areas were equiaxial. It has also been reported that a GBS angle of 25° occurs with 50% deformation.[4,24,31]

In the present study, we found that (1) the contribution ratio of intragranular deformation in the specimens after 50% deformation was 33.5% in the 473 K samples; (2) although θ had a very small value of 4.3°, GBS was likely; and (3) TEM observations showed the presence of subgrains with dislocations and the formation of equiaxial grains after fracture was confirmed in addition to elongated grains. From these findings, the contribution ratio of intragranular deformation is considered to be greater than the deformation mechanism of superplasticity reported.[16–20] In comparison with the reports of Sakai *et al.*,[4,30] our results show a very small amount of sliding ($\theta = 4.3^\circ$) and no agreement with their results except for the rotation of subgrains. Even when the specimens were subjected to 150% deformation, grains in the observed area were mostly elongated in the 473 K samples.

Kobayashi *et al.* reported[22] that when Al-Mg alloy was compressed at 473 K and the total rolling reduction ratio was 90%, the recrystallization temperature decreased to about 553 K, a reduction of 20 to 30 K, as the amount of alloy to be compressed increased. This is because with a higher working ratio and at a lower working temperature, a greater number of dislocations occurred as a result of working, and in turn a greater driving force of recrystallization was created. There is still a difference of about 80 K between the recrystallization temperature mentioned above and the test temperature of 473 K. Thus, it is not logical to conclude that the entire specimen is recrystallized, although the possibility of recrystallization in localized areas cannot be denied. Our results showed that the material had dislocations in the grains, and equiaxial grains were locally observed, even though the specimen was furnace-cooled after fracture. At the same time, as shown in Fig. 6(c), grain boundaries inside elongated grains, including dislocations, began to be formed. On the other hand, as shown in Fig. 7, equiaxial subgrains and subgrains began to be formed locally, with a grain size of 0.9 μm (as identified by the arrows in the figure). The formation of such fine grains as shown by the arrows in Fig. 6(b) is deduced to occur by means of the following process: equiaxial subgrains have a relatively higher density of dislocations than other crystal grains; fine subgrains were formed locally during tensile deformation, and were in turn affected by the rearrangement and disappearance of dislocations caused by recovery during furnace-cooling; and such recovery increased the grain boundary misorientations in the entire specimen and locally formed high-angle grain boundaries, that is, recrystallized grains. We were, however,

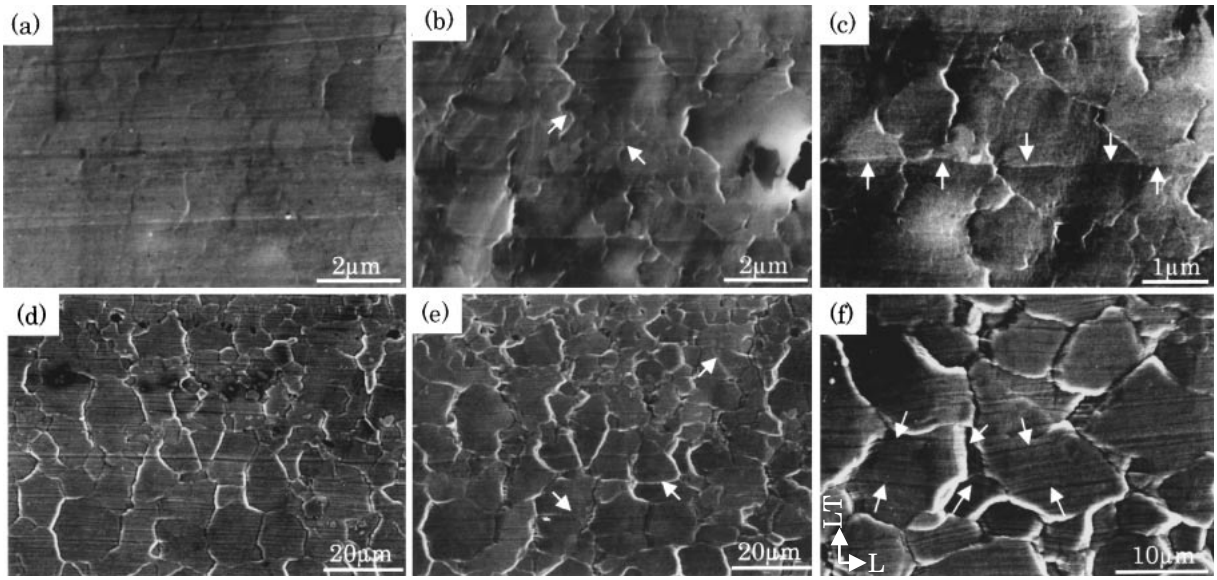

Fig. 9 SEM microstructures of the specimen surface deformed with strain rate of $2.8 \times 10^{-3}\,s^{-1}$ at (a)-(c) 473 K and (d)-(f) 673 K. Elongated to (a),(d) 10% and (b)-(c),(e)-(f) 50%.

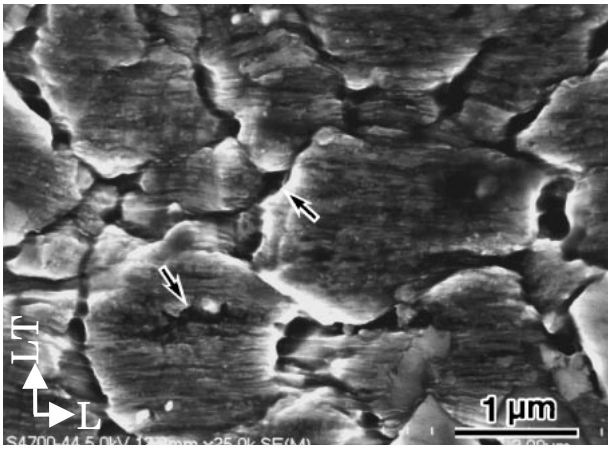

Fig. 10 High resolution SEM microstructure of the 50% deformed specimen surface with strain rate of $2.8 \times 10^{-3}\,s^{-1}$ at 473 K.

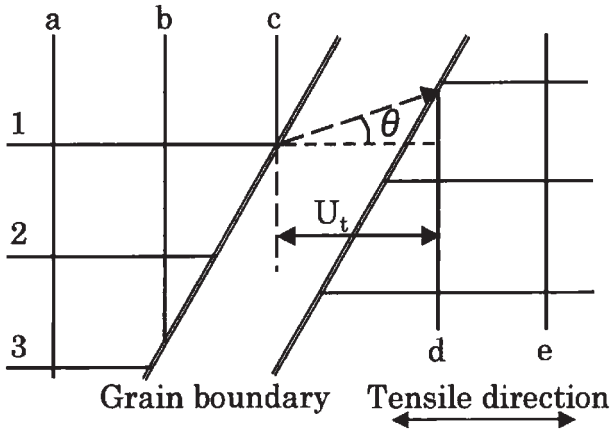

Fig. 11 Schematic representation of rotation angle θ between two grains.

unable to observe static or dynamic or otherwise detailed phenomena in terms of recovery and recrystallization.

In the 673 K samples, marked GBS occurred during deformation at $\theta = 25^{\circ}$, and the grain size increased from 10 to 25 μm after deformation. On the other hand, as shown in Fig. 9(d), surface irregularities occurred in the specimen upon 10% deformation, indicating local formation of finer crystal grains in contrast to surrounding crystal grains. At the same area, after 50% deformation (Fig. 9(e)), it was observed that fine grains had formed around the irregularities on the surface and new grain boundaries had been created in some places (marked by the arrows in the figure). In the 673 K samples, despite the formation of fine grains, grains grew in size after deformation. This phenomenon agrees with the conclusion of the previous reports[11–14] that grain grows with increase of the elongation value in the 673 K samples and that the relationship between elongation and grain size is proportional. It is probable that fine grains were formed, but still grew in size due to the test temperature higher than the recrystallization temperature of the Al-Mg alloy. That is, given the fact that grains grew after the test and their shape was equiaxial, it is inferred that the crystal grain coarsening effect has a major impact on the deformation mechanism of the 673 K samples, as well as on GBS and dynamic recrystallization. From these results, with regard to the appearance of LTSP in ultrafine grains, it is concluded that the change in the microstructure and the deformation mechanism vary according to the test temperature and that it is feasible to realize superplasticity at 473 K, far below 673 K.

4.3 Difference in fracture surface associated with tensile deformation

Figures 12(a) to (d) are SEM microstructure of the top surface and fracture surface of the specimens fractured at $\dot{\varepsilon} = 2.8 \times 10^{-3}\,s^{-1}$. In the 473 K samples, voids elongated in the tensile direction are shown in Fig. 6. As indicated by (a), it is considered that equiaxial voids 2 μm in diameter elongated and connected to their neighboring voids. At the

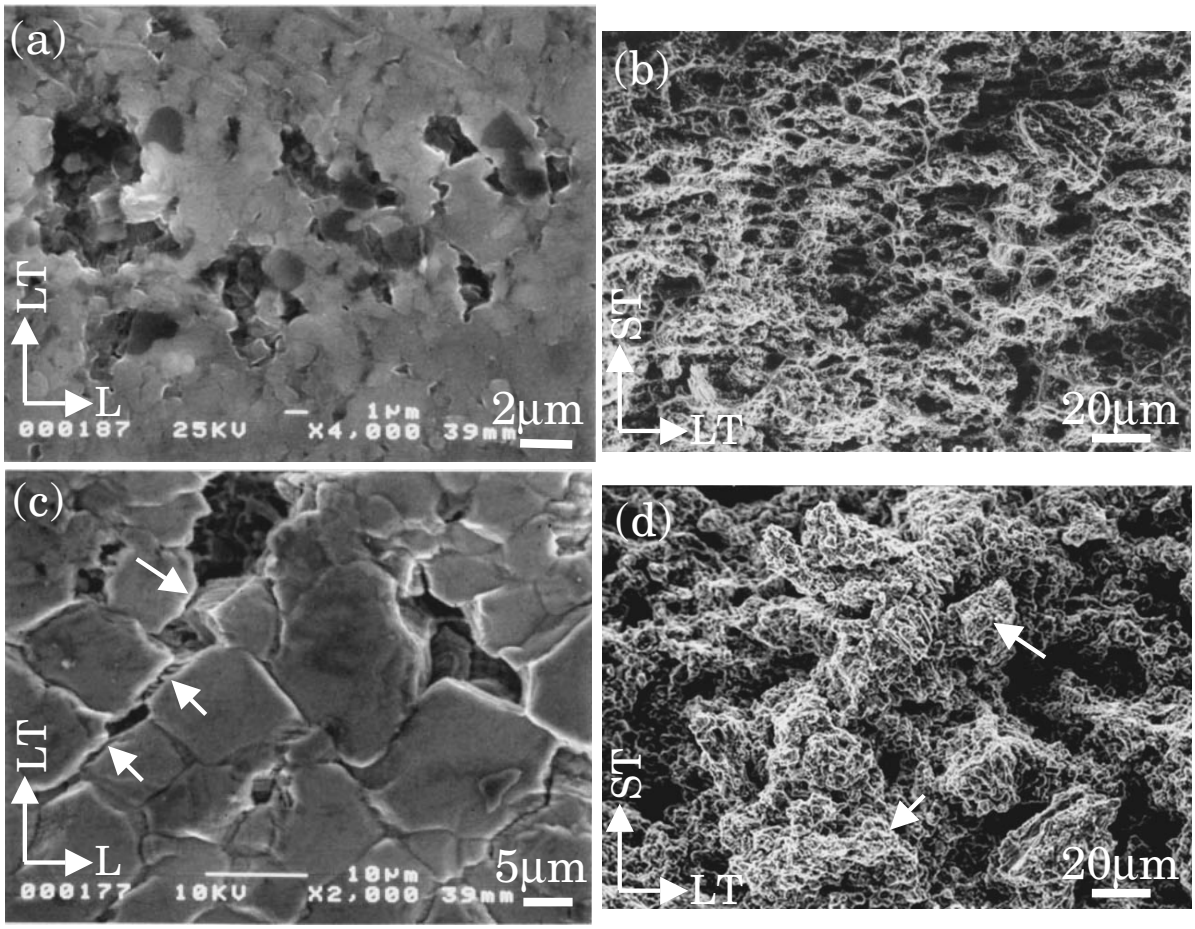

Fig. 12 Fracture surface of specimens tested at strain rate $2.8 \times 10^{-3}\,s^{-1}$. (a),(b) 473 K and (c),(b) 673 K.

same time, no cracks along the grain boundaries or signs of large GBS were observed, so the formation of voids in the 473 K samples are inferred to have been affected by intragranular deformation. In the 673 K samples, 62 μm-diameter voids were observed over the entire test specimen surface. As seen in Fig. 6, cracks generated from equiaxial voids spread along the grain boundaries and combined with other voids in the width direction of the test specimen, as indicated by (c). It is deduced that stress concentration at the triple point of the grain boundary formed by GBS was not mitigated, resulting in generation of these cracks.

Dimples were observed on the fracture surfaces of the 473 K samples, as shown in (b), and no granular irregularities identified by the arrows in (d) occurred. The fracture surfaces in the 473 K samples were similar as the microstructure after deformation under the influence of dislocational movement.[5,32] This corresponds to such findings as the contribution of the above-mentioned intragranular deformation and curved scratches in elongated grains, including dislocations. The fracture surfaces in the 673 K samples shown in (d) indicate granular irregularities of about 10 μm in diameter among large irregularities over the entire surface. It is reported that this form is granularized by surface energy as the driving force and that it is an effect of high-temperature deformation combined with active diffusion.[32] Thus, the form of fracture surface varies depending on the deformation mechanism, and the results obtained for the 473 K samples provide evidence that dislocational movement underwent dominant deformation during the process to fracture.

5. Conclusion

The deformation mechanism of low temperature superplasticity and change of microstructure were investigated in ultrafine grain Al-Mg alloy produced by MAF process. The following results were obtained:

(1) The specimens were heated and maintained at the test temperature of 473 K and 673 K, the ultrafine grains grew to 0.8 μm and 10 μm, respectively.

(2) Under the test conditions of 473 K and a strain rate of $2.8 \times 10^{-3}\,s^{-1}$, an m-value of 0.39 and total elongation of 340% were obtained. These large values indicate the appearance of superplasticity at lower temperatures, which is a characteristic of ultrafine grains.

(3) The mode of void formation varies depending on the test temperature. Elongated voids were formed in the 473 K samples, while equiaxial voids were formed in the 673 K samples.

(4) Tensile test was carried out at the test temperatures of 473 K and 673 K and a strain rate of $2.8 \times 10^{-3}\,s^{-1}$, the contribution ratio of intragranular deformation was 33.5% and 14.4%, respectively, and the grain boundary sliding angle θ was 4.3° and 25°, respectively.

(5) The major deformation mechanism is intragranular

deformation in the 473 K samples and grain boundary sliding in the 673 K samples.

REFERENCES

1) M. Mabuchi, H. Iwasaki, K. Yanase and K. Higashi: Scr. Mater. **36** (1997) 681-686.
2) R. Z. Valiev, N. A. Kraslinikov and N. K. Tsenev: Mater. Sci. Eng. **A137** (1991) 35-40.
3) M. Kawazoe, T. Shibata and K. Higashi: Mater. Sci. Forum **233-234** (1997) 207-214.
4) X. Yang, H. Miura and T. Sakai: J. Japan Inst. Metals **59** (1995) 1222-1229.
5) T. Fujita, S. Komura, Z. Horita and T. G. Langdon: J. JILM **50** (2000) 376-380.
6) R. Kaibyshev, T. Sakai, F. Musin, I. Nikulin and H. Miura: Scr. Mater. **45** (2001) 1373-1380.
7) Z. Horita, S. Lee, S. Ota, K. Neishi and T.G. Langdon: Mater. Sci. Forum **357-359** (2001) 471-476.
8) N. Tsuji, K. Shitotsuki and Y. Saito: Mater. Trans., JIM **40** (1999) 765-771.
9) K. Funami, R. Sano: *4th Pacific Rim Int. Conf. on Advanced Materials and Processing*, (Japan Inst. Metals, 2001) 1983-1986.
10) T. Ohnishi, K. Higashi and Y. Nakatani: J. Japan Inst. Metals **48** (1984) 977-982.
11) H. Iwasaki, T. Mori, M. Mabuchi and K. Higashi: Mater. Sci. Techn. **15** (1999) 180-184.
12) B.M. Watts and M.J. Stowell: J. Mater. Sci. **6** (1971) 228-237.
13) C.H. Caceres and D.S. Wilkinson: Acta Metall. **32** (1984) 415-422.
14) B.P. Kashyap: J. Mater. Sci. **26** (1991) 4657-4662.
15) R.H. Bricknell and J.W. Edington: Met. Trans. **7A** (1976) 153-155.
16) K. Higashi, M. Mabuchi and T.G. Langdon: ISIJ Intl. **36** (1996) 1423-1438.
17) T.G. Langdon: Mater. Sci. Eng. **A174** (1994) 225-230.
18) K. Matsuki, N. Hariyama and M. Tokizawa: J. Japan Inst. Metals **45** (1981) 931-941.
19) Y. Takayama, T. Tozawa, H. Kato, N. Furushiro and S. Hori: Trans. JIM **27** (1986) 416-424.
20) K. Matsuki, Y. Ueno and M. Yamada: J. Japan Inst. Metals **38** (1974) 219-226.
21) M. Noda, M. Hirohashi, K. Funami and Y. Suwahara: J. Japan Inst. Metals **66** (2002) 101-108.
22) M. Kobayashi, K. Funami: *Proc. of the third sympo. on Super Metal* (JRCM, 2001) pp 169-173.
23) Y. Takayama: J. Japan Inst. Light Metals **44** (1994) 48-56.
24) X. Yang, T. Sakai and H. Miura: J. Japan Inst. Light Metals **49** (1999) 383-388.
25) D. Lee: Acta Metall. **17** (1969) 1057-1069.
26) S. Ishihara, T. Tanizawa, K. Akashiro, N. Furushiro and S. Hori: J. Japan Inst. Metals **63** (1999) 333-340.
27) W.A. Rachinger: J. Inst. Metals **81** (1952) 33-41.
28) Y. Ishida, A. W. Mullendore and N.J. Grant: Trans. Met. Soc. AIME **233** (1965) 1648-1650.
29) R.N. Stevens: Trans. Met. Soc. AIME **236** (1966) 1762-1764.
30) H. Gudmundsson, D. Brooks and J. A. Wert: Acta Metall. Mater. **39** (1991) 19-35.
31) T. Sakai: *New approach to grain refinement*, Japan Inst. Metals Seminar Text (The Japan Inst. of Metals, 2000) 83-86.
32) Y. Takayama, S. Sasaki, T. Tozawa, H. Kato, H. Wtanabe and M. Kokubo: J. Japan Inst. Metals **49** (1999) 378-382.